

# Multiscale simulation method for self-organization of nanoparticles in dense suspension

M. Fujita \*, Y. Yamaguchi

*Department of Chemical System Engineering, School of Engineering, The University of Tokyo, Hongo 7-3-1, Bunkyo-ku, Tokyo 113-8656, Japan*

Received 18 August 2005; received in revised form 4 July 2006; accepted 4 September 2006

Available online 17 October 2006

---

## Abstract

This paper presents a multiscale simulation method for self-organization of nanoparticles in a dense suspension. The method consists of a solid–liquid two-phase model, in which the flow of solvent and the motion of nanoparticles are treated by an Euler–Lagrange hybrid scheme with a dual time stepping. The method also includes various multiscale forces whose characteristic length and time scales are much different with one another. Especially frictional force between nanoparticles is included to describe dynamics of aggregated nanoparticles more precisely. Two-dimensional simulation results indicate that the present multiscale method is effective for modeling of motion of nanoparticles in the dense suspension and provides more rational results for self-organization of nanoparticles than previous simulation methods.

© 2006 Elsevier Inc. All rights reserved.

MSC: 65L05; 65M06; 70E55; 76T20; 76D07

*Keywords:* Nanoparticle; Self-organization; Multiscale forces; Frictional force between nanoparticles; Solid–liquid two-phase flow; Euler–Lagrange hybrid scheme

---

## 1. Introduction

In materials nanotechnology, self-organization of nanoparticles is a key technology to fabricate nanoscale structures that have some new mechanical, electrical or optical features. Among the processes for organizing nanoparticles, coating–drying process is preferred for its efficiency in production. In the process, a nanoparticle suspension is coated on a solid substrate and self-organization of nanoparticles take places during drying of the solvent. Fig. 1 shows nanoparticles in a dense suspension just before drying up on a substrate. The self-organization is due to interactions between nanoparticles and interactions between nanoparticles and interfaces [1–4]. It is a nonequilibrium process because the suspension flows and dries, and nanoparticles are subject to various multiscale forces whose characteristic length and time scales are much different with one

---

\* Corresponding author. Tel.: +81 3 58417677; fax: +81 3 58417679.

E-mail address: [masahiro@chemsys.t.u-tokyo.ac.jp](mailto:masahiro@chemsys.t.u-tokyo.ac.jp) (M. Fujita).

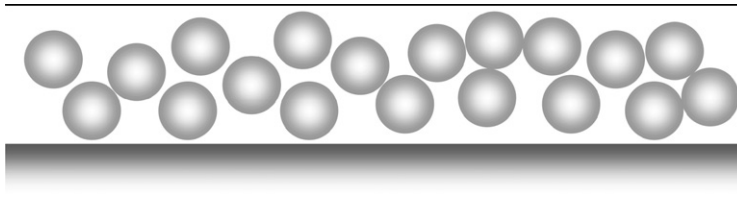


Fig. 1. Nanoparticles in a dense suspension just before drying up on a substrate.

another. Therefore, it is a major challenge to clarify the mechanism of self-organization of nanoparticles in the process.

It is difficult to obtain the dynamic mechanism of self-organization by existing experimental methods. In contrast, numerical simulation is expected to be an effective methodology, because the motion of nanoparticles is visualized with time and the structure of nanoparticles can be quantitatively evaluated. Maenosono et al. developed a two-dimensional numerical model [5] based on molecular dynamics for particles [6–8] to deal with the motion of submicron-sized particles in a suspension during drying. The model included solid contact force, fluid drag force and lateral capillary force [9] that is exerted on semi-immersed particles on a substrate. The simulated monolayer structure of particles was in good qualitative agreement with the corresponding experimental result. Nishikawa et al. developed an improved model [10] that included a periodic boundary condition. They showed that the effect of coverage ratio on the monolayer structure of particles. Recently, we have extended the above method for nano-sized particles in a suspension [11] by introducing Brownian force and forces in the Derjaguin–Landau–Verwey–Overbeek (DLVO) theory [12]. The method includes multiscale forces, such as solid contact force, Brownian force, electrostatic force, van der Waals force, fluid drag force and lateral capillary force. All the forces are essential in the case of nanoparticles, because any force can be the primary force depending on interparticle distance.

In spite of the qualitatively reasonable results [5,10,11], quantitative accuracy of nanoparticle dynamics is not expected for a dense suspension. When the suspension dries and condenses, the distances between nanoparticles in the suspension become small and the Stokes model of fluid drag for each nanoparticle loses its validity, because the effect of the lubrication flow near the gap between nanoparticles becomes prominent. Thus, it is important to introduce a numerical model that is able to count accurately fluid dynamic interactions between nanoparticles in a dense suspension. Solid–liquid two-phase models to describe fluid dynamic interactions have been presented in previous studies [13–17]. The simulation methods of Refs. [13–16] contain Euler–Lagrange hybrid schemes, in which the fluid flow is solved by an Eulerian scheme and the particle motion is solved by a Lagrangian scheme. Takiguchi [13] applied the method to a dilute suspension in which solid contact interactions between particles are not considered. The simulation methods of Refs. [14–16] include only an elastic repulsive force in the normal direction at the contact point as the solid contact interaction between particles. On the other hand, the fluid particle dynamics (FPD) method of Tanaka [17] contains an Eulerian scheme, in which a solid particle is treated as a fluid of high viscosity. The method is rather sophisticated, but friction between particles is not included, and the time step for the fluid flow and that for the particle motion cannot be separated. It is inefficient to use a common time step for the fluid flow and for the particle motion in the case of nanoparticle suspension.

When we take Brownian motion of nanoparticles into consideration as well as fluid dynamic interactions for a dense suspension, the random motion of each nanoparticle should be in principle correlated with those of neighboring particles. There are two approaches to solve this problem. First approach is to apply Brownian–Stokesian dynamics [18–20], in which the variance of the random force exerted on each particle is given by the configuration dependent diffusion tensor. Obtaining the tensor at every time step is a costly operation for a system containing a lot of particles. Second approach is to add fluctuating stresses to the momentum equation of fluid according to the manner by Kramer and Peskin [21] or Sharma and Patankar [22]. The fluctuating stresses for the Navier–Stokes equations are proposed by Landau and Lifshitz [23] at first, and theoretically verified by Fox and Uhlenbeck [24]. This approach may be more efficient than the first approach, because Brownian motion of nanoparticles is caused by the fluctuating fluid force without calculating the diffusion tensor.

The authors here present a multiscale simulation method for self-organization of nanoparticles in a dense suspension. The method consists of a solid–liquid two-phase model, in which the flow of solvent and the motion of nanoparticles are treated by an Euler–Lagrange hybrid scheme. The method also includes a dual time stepping, in which various multiscale forces exerted on each nanoparticle are treated by separate time steps to raise efficiency of calculation. On the basis of molecular dynamics for particles, continuum fluid dynamics and the DLVO theory, the present method includes various multiscale forces whose characteristic length and time scales are much different with one another. Especially frictional force between nanoparticles is included to describe dynamics of aggregated nanoparticles more precisely. The performance of the present method is demonstrated by two-dimensional simulations of flow around a rotating nanoparticle, head-on collision of two nanoparticles and self-organization of many nanoparticles, in which effects of interfaces such as a free surface and a substrate are not included for simplicity.

## 2. Modeling

### 2.1. Motion of nanoparticles

The motion of solid nanoparticles in a dense suspension is solved by a Lagrangian scheme. Each nanoparticle is assumed to be a rigid sphere. The translational motion of the  $k$ -th nanoparticle is expressed by the Langevin Equation

$$m \frac{\partial \mathbf{V}_k}{\partial t} = \mathbf{F}_k, \quad (1a)$$

where

$$\mathbf{F}_k = \mathbf{F}_k^{\text{co}} + \mathbf{F}_k^{\text{ca}} + \mathbf{F}_k^{\text{c}} + \mathbf{F}_k^{\text{v}} + \mathbf{F}_k^{\text{f}} + \mathbf{R}, \quad (1b)$$

$m$  and  $\mathbf{V}$  are the mass and the translational velocity of the nanoparticle, respectively,  $\mathbf{F}_k^{\text{co}}$  is solid contact force,  $\mathbf{F}_k^{\text{ca}}$  is capillary force,  $\mathbf{F}_k^{\text{c}}$  is electrostatic force,  $\mathbf{F}_k^{\text{v}}$  is van der Waals force,  $\mathbf{F}_k^{\text{f}}$  is fluid force and  $\mathbf{R}$  is Brownian random force. Capillary force consists of lateral capillary force and vertical capillary force. Both forces are exerted on a particle that protrudes from a gas–liquid interface, because the interface around the particle is deformed with respect to the contact angle on the particle. The magnitude of lateral capillary attractive force exerted between two homogeneous particles on a substrate is approximated in a simple form [9]. Gravity force and buoyancy force are negligible because the magnitudes of the forces are much smaller than those of other surface forces for nanoparticles.

The trajectory of the  $k$ -th nanoparticle is obtained from the translational velocity as

$$\frac{\partial \mathbf{X}_k}{\partial t} = \mathbf{V}_k, \quad (2)$$

where  $\mathbf{X}_k$  is the position of nanoparticle center. The rotational motion of the  $k$ -th nanoparticle obeys the law of angular momentum conservation

$$I \frac{\partial \boldsymbol{\omega}_k}{\partial t} = \mathbf{T}_k^{\text{co}} + \mathbf{T}_k^{\text{f}}, \quad (3)$$

where  $I$  and  $\boldsymbol{\omega}$  are the inertial moment and the angular velocity of nanoparticle, respectively,  $\mathbf{T}_k^{\text{co}}$  is solid contact torque and  $\mathbf{T}_k^{\text{f}}$  is fluid torque. For a spherical nanoparticle, translational motion of the nanoparticle is unconnected with rotational Brownian motion of the nanoparticle, because the rotational motion does not affect all the forces given in Eq. (1b). In addition, if the nanoparticle contacts with other nanoparticles, the rotational Brownian motion can be suppressed by the solid contact torque. Therefore, we neglect the rotational Brownian motion of nanoparticles here.

The solid contact force and torque act important roles in a dense suspension, because nanoparticles often collide and aggregate with one another and the dynamics of aggregated nanoparticles is strongly affected by the interparticle friction. In almost all previous methods for solid–liquid two-phase flows, the solid contact interactions are treated by a simple elastic repulsion in the normal direction at the contact point between particles [14,15] or the Lennard–Jones potential between particles [16,17]. These treatments are introduced just for

avoiding unphysical overlap between particles, so that it is considered that they cannot appropriately predict the dynamics of aggregated particles. On the other hand, we employ more sophisticated model of solid contact interactions based on the discrete element method [7], in which elastic and damping repulsions in the tangential direction at the contact point between particles are also included as well as those in the normal direction. The present model can describe the slip between particles at the contact point through frictional force. Fig. 2 illustrates the contact between the  $k$ -th sphere and the  $l$ -th sphere. The contact force and torque exerted on the  $k$ -th sphere are obtained by the summation as

$$\mathbf{F}_k^{\text{co}} = \sum_l (\mathbf{F}_{kl}^{\text{n}} + \mathbf{F}_{kl}^{\text{t}}), \quad (4)$$

$$\mathbf{T}_k^{\text{co}} = \sum_l (a \mathbf{n}_{kl} \times \mathbf{F}_{kl}^{\text{t}}), \quad (5)$$

where  $\mathbf{F}^{\text{n}}$  and  $\mathbf{F}^{\text{t}}$  are normal contact force and tangential contact force at the contact point, respectively,  $a$  is the radius of sphere,  $\mathbf{n}_{kl}$  is the unit vector from the center of  $k$ -th sphere to the center of  $l$ -th sphere, and the index  $l$  denotes the neighbors in contact with the  $k$ -th sphere. According to the Voigt model in the field of rheology, the Hertzian contact theory [25] and the Mindlin model [26], normal contact force and tangential contact force are expressed as combinations of elastic and damping forces, respectively,

$$\mathbf{F}_{kl}^{\text{n}} = -k_{\text{n}} \delta_{kl}^{\text{n} 3/2} \mathbf{n}_{kl} - \eta_{\text{n}} (\mathbf{v}_{kl}^{\text{r}} \cdot \mathbf{n}_{kl}) \mathbf{n}_{kl}, \quad (6a)$$

$$\mathbf{F}_{kl}^{\text{t}} = -k_{\text{t}} \delta_{kl}^{\text{t}} - \eta_{\text{t}} \mathbf{v}_{kl}^{\text{t}}, \quad (6b)$$

where

$$\mathbf{v}_{kl}^{\text{t}} = \mathbf{v}_{kl}^{\text{r}} - (\mathbf{v}_{kl}^{\text{r}} \cdot \mathbf{n}_{kl}) \mathbf{n}_{kl} + a(\boldsymbol{\omega}_k + \boldsymbol{\omega}_l) \times \mathbf{n}_{kl}, \quad (6c)$$

$k_{\text{n}}$  and  $k_{\text{t}}$  are elastic coefficients of nanoparticles of normal and tangential direction, respectively,  $\eta_{\text{n}}$  and  $\eta_{\text{t}}$  are damping coefficients of nanoparticles of normal and tangential direction, respectively,  $\delta^{\text{n}}$  and  $\delta^{\text{t}}$  are the normal and tangential relative displacement of the contact point, respectively, and  $\mathbf{v}^{\text{r}}$  is the relative velocity of the contact point. The tangential relative displacement vector at time  $t$  is derived from rotation of that at the previous time step and tangential relative velocity  $\mathbf{v}^{\text{t}}$  as

$$\boldsymbol{\delta}_{kl}^{\text{t}}(t) = |\boldsymbol{\delta}_{kl}^{\text{t}}(t - \Delta t)| \frac{\mathbf{n}_{kl} \times \boldsymbol{\delta}_{kl}^{\text{t}}(t - \Delta t) \times \mathbf{n}_{kl}}{|\mathbf{n}_{kl} \times \boldsymbol{\delta}_{kl}^{\text{t}}(t - \Delta t) \times \mathbf{n}_{kl}|} + \mathbf{v}_{kl}^{\text{t}} \Delta t, \quad (7)$$

because the unit normal vector to the contact plane changes the direction during  $\Delta t$ . According to the law of Coulomb friction, a slip at the contact point is expressed by modifications of Eqs. (6b) and (7) as

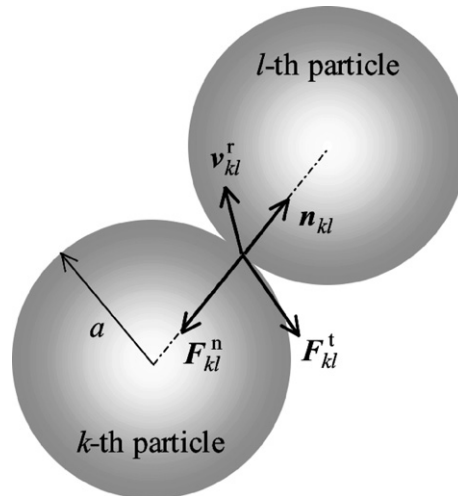


Fig. 2. Contact of two spheres.

$$\mathbf{F}_{kl}^t = -\mu |\mathbf{F}_{kl}^n| \mathbf{t}_{kl}, \quad (8a)$$

$$\delta_{kl}^t = -\mathbf{F}_{kl}^t / k_t, \quad (8b)$$

if

$$|\mathbf{F}_{kl}^t| \geq \mu |\mathbf{F}_{kl}^n|, \quad (8c)$$

where

$$\mathbf{t}_{kl} = \mathbf{v}_{kl}^t / |\mathbf{v}_{kl}^t|, \quad (8d)$$

and  $\mu$  is the frictional coefficient between spheres or between a sphere and a wall. The elastic coefficients in the case of contact between two spheres of the same radius are obtained by the Hertzian contact theory and the Mindlin model as

$$k_n = \frac{\sqrt{2a}E_s}{3(1-\sigma_s^2)}, \quad (9a)$$

$$k_t = \frac{2\sqrt{2a}G_s}{2-\sigma_s} \delta_{kl}^{n\ 1/2}. \quad (9b)$$

The normal and the tangential damping coefficients are assumed to be the same value, which is derived from a restitution coefficient [7] as

$$\eta_n = \eta_t = \lambda(mk_n)^{1/2} \delta_{kl}^{n\ 1/4} \quad (\lambda \sim 1). \quad (10)$$

The electrostatic force exerted between two spheres is treated together with the van der Waals force in the DLVO theory as

$$\mathbf{F}_k^e + \mathbf{F}_k^v = \sum_l (f_{kl}^e + f_{kl}^v) \mathbf{n}_{kl}. \quad (11)$$

The magnitude of electrostatic repulsive force exerted on two homogeneously charged spheres is derived through Derjaguin's approximation [12] as

$$f_{kl}^e = -\frac{64\pi n a k_b T \Theta^2 e^{-\kappa H_{kl}}}{\kappa}, \quad (12a)$$

where

$$\Theta = \tanh\left(\frac{ze\varphi}{4k_b T}\right), \quad (12b)$$

$$\kappa = \sqrt{\frac{2nz^2e^2}{\varepsilon_0\varepsilon_r k_b T}}, \quad (12c)$$

and  $n$  is the number density of electrolyte ions,  $k_b$  is boltzmann constant,  $T$  is the temperature of suspension,  $H$  is the intersurface distance between spheres,  $z$  is the electrolyte ionic valency,  $e$  is the elementary electric charge,  $\varphi$  is the zeta potential,  $\varepsilon_0$  is permittivity of vacuum and  $\varepsilon_r$  is the relative permittivity of solvent. The magnitude of van der Waals force is derived through a volume integration of the force exerted between two atoms that are contained in spheres as

$$f_{kl}^v = \frac{Aa}{12H_{kl}^2}, \quad (13)$$

where  $A$  is the Hamaker constant. Note that the magnitude of van der Waals force is limited below a maximum value to prevent divergence of the value when the intersurface distance comes to zero.

Brownian force is exerted on nanoparticles in random directions. As mentioned before, the variance of the random force should be given by the configuration dependent tensor [18] if the Langevin equation for a Brownian particle is used. The authors employ, however, simpler and more efficient model to include Brownian motion in the present method, in which variances of random forces exerted on nanoparticles are identical

to that on single isolated particle as given by the original Langevin equation. This bold model can describe the effects of Brownian motions of nanoparticles on self-organization of the nanoparticles with enough accuracy, although the fluctuation-dissipation theorem is not strictly satisfied. The standard deviation of the distribution of the random force is derived from the original Langevin equation and the law of energy equipartition as

$$\sigma = \sqrt{\frac{6\zeta k_b T}{\Delta t}}, \quad (14)$$

where  $\zeta$  is the coefficient of Stokes drag for a sphere. The models of fluid force and fluid torque are described subsequently.

## 2.2. Flow of solvent

The flow of solvent is solved by an Eulerian scheme on a uniform Cartesian grid. Since the Reynolds number of the flow is less than 1, the equation of motion is given by the Stokes equation

$$\frac{\partial \mathbf{u}}{\partial t} = -\frac{1}{\rho} \nabla p + \nu \nabla^2 \mathbf{u} + \mathbf{a}, \quad (15)$$

where  $\mathbf{u}$  is the fluid velocity,  $\rho$  is the density,  $p$  is the pressure,  $\nu$  is the dynamic viscosity and  $\mathbf{a}$  is fluid acceleration due to motion of particles. Each particle is embedded on the Cartesian grid and the fluid acceleration works only inside particles to force the particle velocity on grid points. This is a type of immersed-boundary approach [27]. The fluid acceleration is given by

$$\mathbf{a} = \Phi \left( \frac{\mathbf{u}^p - \mathbf{u}}{\Delta t} - \nu \nabla^2 \mathbf{u} \right), \quad (16a)$$

where

$$\Phi = \sum_k \phi_k(\mathbf{r}), \quad (16b)$$

$\mathbf{u}^p$  is the particle velocity on grid points and  $\phi_k(\mathbf{r})$  is the concentration field of the  $k$ -th particle. When each particle is a sphere, the concentration field is given by a hyperbolic tangent function [16,17] as

$$\phi_k(\mathbf{r}) = \frac{1}{2} \left\{ \tanh \left( \frac{a - |\mathbf{r} - \mathbf{r}_k|}{\zeta} + 1 \right) \right\}, \quad (17)$$

where  $\mathbf{r}$  is position vector of grid points,  $\mathbf{r}_k$  is the position vector of center of  $k$ -th particle and  $\zeta$  determines the thickness of particle–fluid interface. The value of Eq. (17) smoothly changes from 0 to 1 through the interface. In the present study,  $\zeta$  is set to 0.025 so that thickness of the interface is represented by twice the grid spacing. Although there are various methods for tracking of solid–fluid interface such as the level set method [28] or the method using constrained interpolation profile (CIP) [29], we use the Lagrange scheme that is formulated to deal with the motion of particles. In a word, a particle concentration field moves with time according to Eq. (2). This simple method to specify moving solid particles in a fluid is more efficient and robust than any other methods that contain solution-interpolation procedures on solid–fluid interface, such as Ref. [13]. The particle velocity term in Eq. (16) is expressed by

$$\Phi \mathbf{u}^p = \sum_k \{ \phi_k(\mathbf{r}) (\mathbf{v}_k + (\mathbf{r} - \mathbf{r}_k) \times \boldsymbol{\omega}_k) \}. \quad (18)$$

Using the fluid acceleration, the diffusion term in Eq. (15) vanishes inside particles.

Based on the assumption of rigid body, the pressure inside particles are averaged and the constant pressure of the  $k$ -th nanoparticle is calculated at every time step as

$$p_k^p = \frac{\int \phi_k(\mathbf{r}) p(\mathbf{r}) d\mathbf{r}}{\int \phi_k(\mathbf{r}) d\mathbf{r}}, \quad (19)$$

where the integration is done in the region surrounding the nanoparticle. Then the pressure field is modified as

$$p(\mathbf{r}) = p(\mathbf{r}) + \sum_k [\phi_k(\mathbf{r})\{p_k^p - p(\mathbf{r})\}]. \quad (20)$$

This pressure averaging eliminates the pressure gradient term in Eq. (15) inside particles. By using Eqs. (16) and (20) with Eq. (15), the particle velocity  $\mathbf{u}^p$  is automatically forced on the velocity field inside particles at the next time step. The present solid–liquid two-phase model resembles direct forcing method [30] except using the particle concentration field and the pressure averaging. An advantage of the present immersed-boundary approach using Eqs. (16) and (20) is that the fluid force in Eq. (1) and the fluid torque in Eq. (3) are directly derived from the fluid acceleration through volume integrations as

$$\mathbf{F}_k^f = - \int \phi_k(\mathbf{r}) \rho \mathbf{a}(\mathbf{r}) d\mathbf{r}, \quad (21)$$

$$\mathbf{T}_k^f = - \int \phi_k(\mathbf{r}) \{(\mathbf{r} - \mathbf{r}_k) \times \rho \mathbf{a}(\mathbf{r})\} d\mathbf{r}. \quad (22)$$

Using Eqs. (15), (21) and (22), the law of momentum conservation between solid and liquid can be adequately satisfied.

### 2.3. Solution algorithm

Eq. (15) with the incompressibility condition  $\nabla \cdot \mathbf{u} = 0$  is solved by a finite difference method. The method, unlike a spectral method, is applicable to a variety of practical configurations and boundary conditions. Eq. (15) is temporally discretized by Crank-Nicolson scheme and solved by a combination of tridiagonal matrix algorithm (TDMA) and line successive over relaxation algorithm (line-SOR). The Poisson equation of pressure is solved by highly simplified marker and cell (HSMAC) scheme [31]. On the other hand, Eq. (1) and (3) are temporally discretized by Euler explicit scheme, and the position and the rotational angle of nanoparticles are obtained by Crank-Nicolson scheme. Although the motion of nanoparticle is solved by the Lagrange scheme, a computational region is divided into a number of unit cells. Index of the cell in which center of each nanoparticle is contained, is obtained at the beginning of every time step. The cell index for each nanoparticle can remarkably reduce the computational cost to find counterpart nanoparticles with which contact force, electrostatic force and van der Waals force are exerted. Fig. 3 shows a relationship between cells for Lagrangian scheme and grid for Eulerian scheme with reference to a nanoparticle. The diameter of a nanoparticle contains 9 grid points in the case of normal grid.

The multiscale forces exerted on a nanoparticle are classified into two categories with respect to the characteristic length and time scales. The scales of contact force, electrostatic force and van der Waals force are

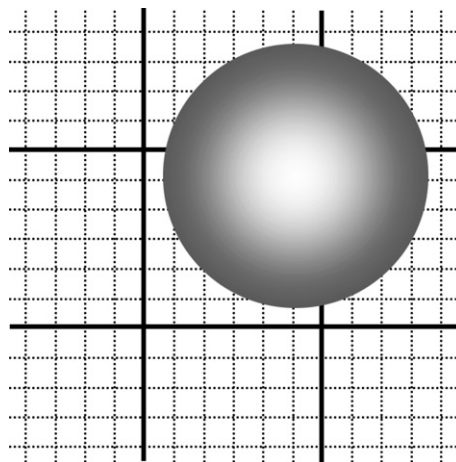


Fig. 3. Relationship between cells for Lagrangian scheme (solid line) and grid for Eulerian scheme (dashed line) with reference to a nanoparticle.



associated with the motion of molecules in the nanoparticles or the solvent. On the other hand, the scales of Brownian force and fluid force are associated with the motion of nanoparticle. If a common time step is used to calculate every force, the time step is limited to the scale associated with the molecular motion and the computational cost inevitably increases because solving Eq. (15) is expensive. Thus, a dual time stepping is introduced here. In particular,  $\mathbf{F}_k^{\text{co}}$ ,  $\mathbf{F}_k^{\text{c}}$ ,  $\mathbf{F}_k^{\text{v}}$  in Eq. (1) and  $\mathbf{T}_k^{\text{co}}$  in Eq. (3) are calculated at a small time step  $\Delta t_s$ , and  $\mathbf{F}_k^{\text{f}}$ ,  $\mathbf{R}$  in Eq. (1) and  $\mathbf{T}_k^{\text{f}}$  in Eq. (3) are calculated at a large time step  $\Delta t_l$ . Then Eq. (15) is solved at  $\Delta t_l$  and

$$\Delta t_l = n\Delta t_s, \quad (23)$$

where  $n$  is a positive integer.

### 3. Simulation results

The authors demonstrate performance of the present simulation method by two-dimensional simulations, in which effects of interfaces such as a free surface and a substrate are not included in order to focus on the effects of a combination of molecular dynamics, continuum fluid dynamics and the DLVO theory. Hence capillary force between nanoparticles, and solid contact force/torque between nanoparticles and a substrate in Eqs. (1) and (3) are not taken into consideration here.

#### 3.1. Flow around a rotating nanoparticle

Before consideration is given to a self-organization of nanoparticles, the present solid–liquid two-phase model is verified by calculating flow around a rotating nanoparticle in a still fluid. A circular nanoparticle with a diameter of 50 nm is fixed in a computational region and rotates with a prescribed angular velocity. The flow is expressed by an analytical solution of two-dimensional circular vortex under theory of Stokes flow as

$$v_\theta(r) = \begin{cases} \Omega r & r \leq a \\ \Omega a^2/r & r > a \end{cases}, \quad (24)$$

where  $v_\theta$  is circumferential velocity,  $r$  is the distance from the center of nanoparticle and  $\Omega$  is the angular velocity of nanoparticle. Fig. 4 shows a simulated velocity field near a rotating nanoparticle when  $\Omega = 1$ . It is shown that the rigid rotational velocity is forced on grid points inside the nanoparticle, and it induces a rotative flow outside the nanoparticle. Non-slip boundary condition on the nanoparticle surface is well satisfied although the grid points do not coincide with the surface. Fig. 5 shows the magnitude of circumferential velocity as a function of the distance from the nanoparticle center. Although computational result on normal grid, in which 9 grid points are contained in the diameter of nanoparticle, is rather similar to the analytical solution of Stokes theory throughout the distance, it slightly underestimates the circumferential velocity in the region

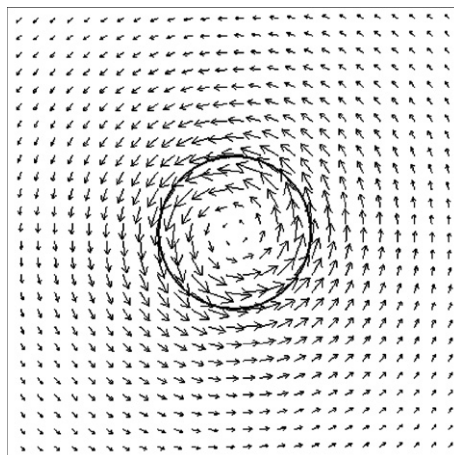


Fig. 4. Velocity field around a rotating nanoparticle in a still fluid.



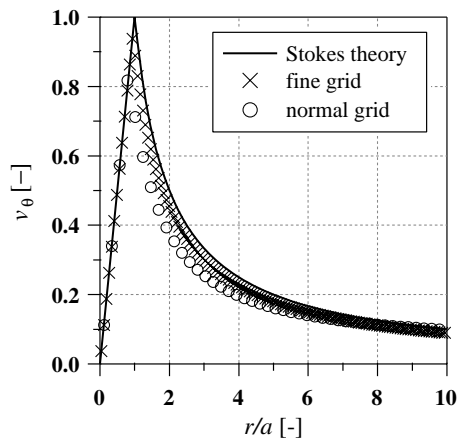


Fig. 5. Magnitude of circumferential velocity as a function of distance from nanoparticle center on the normal grid ( $2a = 9\Delta$ ) and on the fine grid ( $2a = 27\Delta$ ), where  $\Delta$  is grid spacing.

just outside the nanoparticle. The reason of this discrepancy is that the maximum circumferential velocity at nanoparticle surface is not exactly captured in the computational result due to a lack of grid resolution. This point is justified by the fact that computational result on fine grid, in which 27 grid points are contained in the diameter of the nanoparticle, agrees well with the Stokes theory as shown in Fig. 5. One can say that the present solid–liquid two-phase model gives accurate solution depending on a grid resolution.

### 3.2. Head-on collision of two nanoparticles

Whereas Section 3.1 served to demonstrate the correctness of the present Euler–Lagrange scheme without Brownian and DLVO forces, we now include these forces for a two particle system as follows: Two homogeneous circular nanoparticles whose diameter is 50 nm and zeta-potential are  $-100$  mV advance towards each other in alignment with a prescribed velocity of 0.1 in a still fluid. The physical and chemical properties of the nanoparticles and the fluid are given by the same values as those of polystyrene and water in normal temperature, respectively. Fig. 6 shows a simulated velocity field around two nanoparticles on the normal grid when an intersurface distance between them is equal to the diameter of nanoparticles. It is shown that the rigid translational velocity is forced on grid points inside the nanoparticles and an outward cross-flow is induced between the nanoparticles.

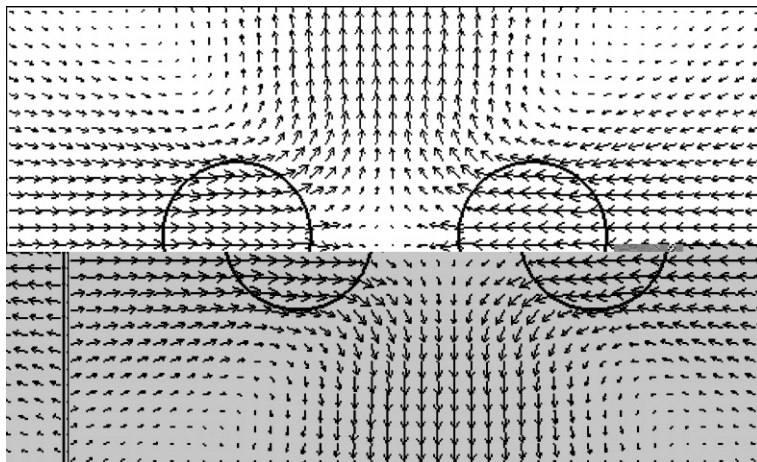


Fig. 6. Velocity field around two nanoparticles that advance towards each other in a still fluid.

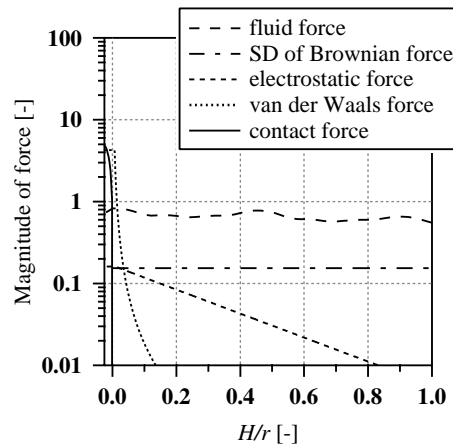


Fig. 7. Magnitudes of nondimensional forces exerted on nanoparticles that advance towards each other as a function of intersurface distance between them.

Fig. 7 shows the magnitudes of nondimensional forces exerted on nanoparticles as a function of intersurface distance between them. When there is enough distance between two nanoparticles, Brownian force and fluid force that naturally depends on the velocity of nanoparticles are distinguished among every force, because they are interactions between a nanoparticle and a solvent. As the distance between the nanoparticles becomes reduced, electrostatic force that is a long-ranged two-body force exerts a considerable effect on the nanoparticles. Just before a collision of two nanoparticles, van der Waals attractive force that is a short-ranged two-body force rapidly increases and becomes the strongest force among every force. After a collision of two nanoparticles, contact repulsive force is exerted on nanoparticles and matches well with van der Waals attractive force. Consequently, the magnitude relation of forces exerted on the nanoparticles remarkably changes with the intersurface distance between them, so that every force in molecular dynamics, continuum fluid dynamics and the DLVO theory are indispensable for modeling of nanoparticles in a dense suspension.

### 3.3. Self-organization of many nanoparticles

The authors finally present a simulation result of two-dimensional self-organization of many nanoparticles. Computational conditions are chosen as follows: a computational region is a square with a side length of  $1.35\ \mu\text{m}$ , which contains  $40 \times 40$  cells for the Lagrangian scheme and  $240 \times 240$  normal grid for the Eulerian scheme. A diameter of circular nanoparticles is  $50\ \text{nm}$ , the zeta-potential of the nanoparticles is  $-10\ \text{mV}$  and the frictional coefficient of particle-to-particle is  $0.1$ . Other physical and chemical properties of nanoparticles and the solvent are given by the same values as those of polystyrene and water in normal temperature, respectively. The coverage ratio, which is 1 if the entire computational region is covered with hexagonally close-packed nanoparticles, is set to  $0.5$ . Hence the number of particles is  $420$ . A periodic boundary condition is imposed on four sides of the computational region. Time steps for the dual time stepping are  $\Delta t_s = 0.01\ \text{ns}$  and  $\Delta t_l = 0.1\ \text{ns}$ , respectively.

Self-organization process of nanoparticles in the suspension obtained by the present simulation method is shown in Fig. 8. Nanoparticles are randomly dispersed in the suspension at the beginning of simulation, as shown in Fig. 8(a). After start of the simulation, nanoparticles locally form chain-like clusters, as shown in Fig. 8(b), which is mainly due to Brownian motion of nanoparticles and van der Waals attractive force exerted between close nanoparticles. As time goes on, the clusters attract neighboring nanoparticles and increase in size, as shown in Fig. 8(c). Finally, the chain-like clusters coalesce with one another and form a network structure throughout the computational region, as shown in Fig. 8(d). On the other hand, simulation results obtained by Stokes drag model and no-friction model are shown in Fig. 9. Fig. 9(a) shows the simulation result in which fluid force is modeled by theorem of Stokes drag without solving the flow of solvent. It is essentially a conventional Brownian dynamics simulation with the sophisticated solid contact model. Effect of fluid

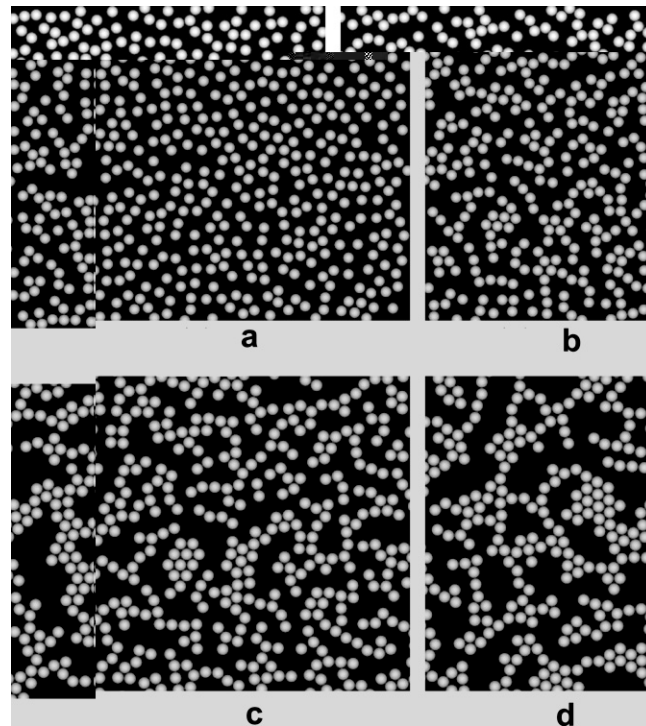


Fig. 8. Self-organization process of nanoparticles in the suspension obtained by the present method: (a)  $t = 0 \mu\text{s}$ ; (b)  $t = 2.5 \mu\text{s}$ ; (c)  $t = 5 \mu\text{s}$ ; (d)  $t = 10 \mu\text{s}$ .

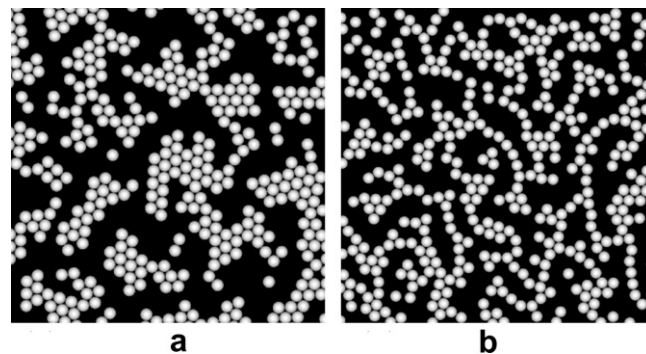


Fig. 9. Simulation results obtained by stokes drag model and no-friction model ( $t = 10 \mu\text{s}$ ): (a) Stokes drag model; (b) no-friction model.

dynamic interactions between nanoparticles can be clearly recognized by comparing this figure with Fig. 8(d). Without the fluid dynamic interactions, nanoparticles do not form chain-like clusters but form locally agglomerated clusters, so that an island structure of nanoparticles is generated. It is considered that there are two major fluid dynamic interactions: The first interaction is an interparticle repulsive force due to a high pressure that emerges between oncoming nanoparticles. This repulsive force may inhibit aggregation of nanoparticles in a cluster and generate chain-like clusters. The second interaction is an interparticle attractive force due to a low pressure that emerges between nanoparticles receding from each other. This attractive force may accelerate coalescence of neighboring clusters and generate a network structure. Fig. 9(b) shows the simulation result in which particle-to-particle friction is not modeled. Effect of frictional interactions can be recognized by comparing this figure with Fig. 8(d). Although network structures of nanoparticles are found in both figures, chain-like clusters and resultant network structure in Fig. 9(b) are finer than those in Fig. 8(d). Without

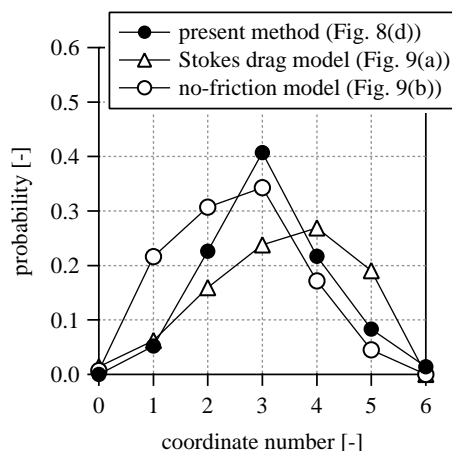


Fig. 10. Probability distribution of number of nanoparticles as a function of coordinate number obtained by the present method, Stokes model and no-friction model ( $t = 10 \mu\text{s}$ ).

the frictional interactions, each chain-like cluster of nanoparticles easily transforms its shape according to fluid dynamic interactions with the surrounding solvent. As a result, it is anticipated that clusters hardly collide with one another and a fine network is generated.

Difference among simulation results by the present method, Stokes model and no-friction model is quantitatively indicated in Fig. 10. This figure shows the probability distribution of number of nanoparticles as a function of coordinate number. The coordinate number is the number of nanoparticles that contact with a nanoparticle. The probability distribution for the simulation result by Stokes model is displaced toward right with respect to the simulation result by the present method, because nanoparticles in agglomerated clusters have larger coordinate numbers than nanoparticles in chain-like clusters. On the other hand, the probability distribution for the simulation result by no-friction model is displaced toward left with respect to the simulation result by the present method, because nanoparticles in fine clusters have smaller coordinate numbers than nanoparticles in coalescent clusters. Consequently, one can say that the present simulation method provides rational results because the method includes fluid dynamic interactions and solid contact interactions that are important for self-organization of nanoparticles in a dense suspension.

#### 4. Conclusion

The authors have developed a multiscale simulation method for self-organization of nanoparticles in a dense suspension on the basis of molecular dynamics, continuum fluid dynamics and the DLVO theory. The conclusions are as follows: firstly, the solid–liquid two-phase model gives accurate solution depending on a grid resolution. Secondly, sophisticated model of solid contact interactions including frictional force between nanoparticles gives more rational result than previous simulation method. Finally, the dual time stepping used here is more efficient than other models using a uniform time step. Although simulation results shown here are limited to two-dimensional, the present method essentially consists of three-dimensional models and three-dimensional applications will be presented in future. It is also expected that the present method can be applied to a shear flow of nanoparticle suspensions during coating processes. The authors believe that the present multiscale simulation method can be a powerful tool to clarify the mechanism of self-organization of nanoparticles in the coating-drying process.

#### References

- [1] N.D. Denkov, O.D. Velev, P.A. Kralchevsky, I.B. Ivanov, H. Yoshimura, K. Nagayama, *Langmuir* 8 (1992) 3183.
- [2] L. Motte, E. Lacaze, M. Maillard, M.P. Pileni, *Langmuir* 16 (2000) 3803.
- [3] S.C. Rodner, P. Wedin, L. Bergstrom, *Langmuir* 18 (2002) 9327.

- [4] T. Okubo, S. Chujo, S. Maenosono, Y. Yamaguchi, *J. Nanopart. Res.* 5 (2003) 111.
- [5] S. Maenosono, C.D. Dushkin, Y. Yamaguchi, K. Nagayama, Y. Tsuji, *Colloid. Polym. Sci.* 277 (1999) 1152.
- [6] P.A. Cundall, O.D.L. Strack, *Geotechnique* 29 (1979) 47.
- [7] Y. Tsuji, T. Tanaka, T. Ishida, *Powder Tech.* 71 (1992) 239.
- [8] L. Popken, P.W. Cleary, *J. Comp. Phys.* 155 (1999) 1.
- [9] P.A. Kralchevsky, K. Nagayama, *Langmuir* 10 (1994) 23.
- [10] H. Nishikawa, S. Maenosono, Y. Yamaguchi, T. Okubo, *J. Nanopart. Res.* 5 (2003) 103.
- [11] M. Fujita, H. Nishikawa, T. Okubo, Y. Yamaguchi, *Jpn. J. Appl. Phys.* 43 (2004) 4434.
- [12] J.N. Israelachvili, *Intermolecular and Surface Forces*, Academic Press, London, 1992.
- [13] S. Takiguchi, T. Kajishima, Y. Miyake, *JSME Int. J. B* 42 (1999) 411.
- [14] W. Kalthoff, S. Schwarzer, H.J. Herrmann, *Phys. Rev. E* 56 (1997) 2234.
- [15] K. Höfler, S. Schwarzer, *Phys. Rev. E* 61 (2000) 7146.
- [16] R. Yamamoto, Y. Nakayama, K. Kim, *J. Phys.: Condens. Matt.* 16 (2004) S1945.
- [17] H. Tanaka, T. Araki, *Phys. Rev. Lett.* 85 (2000) 1338.
- [18] D.L. Ermak, J.A. McCammon, *J. Chem. Phys.* 69 (1978) 1352.
- [19] S.R. Rastogi, N.J. Wagner, *Comput. Chem. Eng.* 19 (1995) 693.
- [20] T.N. Phung, J.F. Brady, G. Bossis, *J. Fluid Mech.* 313 (1996) 181.
- [21] P.R. Kramer, C.S. Peskin, *Comparative Fluid and Solid Mechanics*, in: K.J. Bathe (Ed.), *Proceedings of The Second MIT Conference on Comparative Fluid and Solid Mechanics*, 17–20 June, 2003, Elsevier, Oxford, 2003, p. 1755.
- [22] N. Sharma, N.A. Patankar, *J. Comp. Phys.* 201 (2004) 466.
- [23] L.D. Landau, E.M. Lifshitz, *Fluid Mechanics*, Pergamon Press, London, 1959.
- [24] R.F. Fox, G.E. Uhlenbeck, *Phys. Fluid* 13 (1970) 1893.
- [25] S.P. Timoshenko, J.N. Goodier, *Theory of Elasticity*, McGraw-Hill, New York, 1970.
- [26] R.D. Mindlin, H. Deresiewicz, *J. Appl. Mech.* 20 (1953) 327.
- [27] C.S. Peskin, *Acta Numer.* 11 (2002) 479.
- [28] S. Osher, R.P. Fedkiw, *J. Comp. Phys.* 169 (2001) 463.
- [29] T. Yabe, F. Xiao, T. Utsumi, *J. Comp. Phys.* 169 (2001) 556.
- [30] E.A. Fadlun, R. Verzicco, P. Orlandi, J. Mohd-Yusof, *J. Comp. Phys.* 161 (2000) 35.
- [31] C.W. Hirt, J.L. Cook, *J. Comp. Phys.* 10 (1972) 324.